Inorg. Chem. **2003**, *42*, 3111–3118

Dynamical Intramolecular Metal-to-Metal Ligand Exchange of Phosphine and Thioether Ligands in Derivatives $PtRu_5(CO)_{16}(\mu_6\text{-}C)$

Richard D. Adams,* Burjor Captain, Wei Fu, and Perry J. Pellechia

Department of Chemistry and Biochemistry and USC NanoCenter, University of South Carolina, Columbia, South Carolina 29208

Received December 3, 2002

The complexes $PtRu_5(CO)_{15}(PMe_2Ph)(\mu_6\text{-}C)$ (**2**), $PtRu_5(CO)_{14}(PMe_2Ph)_2(\mu_6\text{-}C)$ (**3**), $PtRu_5(CO)_{15}(PMe_3)(\mu_6\text{-}C)$ (**4**), $PtRu_5(CO)_{14}(PMe_3)_2(\mu_6\text{-}C)$ (**5**), and $PtRu_5(CO)_{15}(Me_2S)(\mu_6\text{-}C)$ **(6)** were obtained from the reactions of $PtRu_5(CO)_{16}(\mu_6\text{-}C)$ (**1**) with the appropriate ligand. As determined by NMR spectroscopy, all the new complexes exist in solution as a mixture of isomers. Compounds **2**, **3**, and **6** were characterized crystallographically. In all three compounds, the six metal atoms are arranged in an octahedral geometry, with a carbido carbon atom in the center. The PMe_2Ph and Me_2S ligands are coordinated to the Pt atom in **2** and **6**, respectively. In **3**, the two PMe_2Ph ligands are coordinated to Ru atoms. In solution, all the new compounds undergo dynamical intramolecular isomerization by shifting the PMe_2Ph or Me_2S ligand back and forth between the Pt and Ru atoms. For compound **2**, $\Delta H^{\ddagger} = 15.1(3)$ kcal/mol, $\Delta S^{\ddagger} = -7.7(9)$ cal/(mol·K), and $\Delta G_{298} = 17.4(6)$ kcal/mol for the transformation of the major isomer to the minor isomer; for compound **4**, $\Delta H^{\ddagger} = 14.0(1)$ kcal/mol, $\Delta S^{\ddagger} = -10.7(4)$ cal/(mol·K), and $\Delta G_{298} = 17.2(2)$ kcal/mol for the transformation of the major isomer to the minor isomer; for compound **6**, $\Delta H^{\ddagger} = 18(1)$ kcal/mol, $\Delta S^{\ddagger} = 21(5)$ cal/(mol·K) and $\Delta G_{298} = 12(2)$ kcal/mol. The shifts of the Me_2S ligand in **6** are significantly more facile than the shifts for the phosphine ligand in compounds **2**–**5**. This is attributed to a more stable ligand-bridged intermediate for the isomerizations of **6** than that for compounds **2**–**5**. The intermediate for the isomerization of **6** involves a bridging Me_2S ligand that can use two lone pairs of electrons for coordination to the metal atoms, whereas a tertiary phosphine ligand can use only one lone pair of electrons for bridging coordination.

Introduction

The ability of polynuclear metal complexes to rearrange their ligand frameworks is central to understanding their reactivity.[1] Today, there are many examples of dynamical processes in polynuclear metal complexes through which ligands exchange sites intramolecularly between metal atoms.[1,2] CO, CNR, and NO ligands are the most common examples of ligands that undergo these exchange processes rapidly. This is due, in part, to the ability of these ligands to coordinate in stable bridging modes, where they are simultaneously bonded to two or more metal atoms. There is only one previous report that demonstrates a facile intramolecular exchange of a phosphine ligand between metal atoms in polynuclear metal complex.[3] Here, we report new evidence on the ability of phosphines and thioether ligands to undergo metal-to-metal ligand exchange *intramolecularly* in derivatives of the mixed-metal cluster complex $PtRu_5(CO)_{16}(\mu_6\text{-}C)$, **1**.[4] A preliminary report of this work has been published.[5]

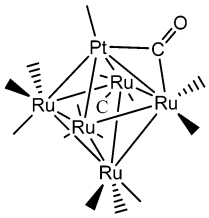

* Author to whom correspondence should be addressed. E-mail: Adams@mail.chem.sc.edu.

(1) (a) Johnson, B. F. G.; Benfield, R. E. In *Transition Metal Clusters*; Johnson, B. F. G., Ed.; Wiley, Chichester, U.K., 1980; Chapter 7. (b) Muetterties, E. L.; Band, E. *Chem. Rev.* **1978**, *78*, 639.

(2) (a) Adams, R. D.; Cotton, F. A. In *Dynamic Nuclear Magnetic Resonance Spectroscopy*; Jackman, L., Cotton, F. A., Eds.; Academic Press: New York, 1975; Chapter 12. (b) Farrugia, L. J.; Orpen, A. G. In *Metal Clusters in Chemistry*; Braunstein, P., Oro, L. A., Raithby, P. R., Eds.; Wiley−VCH: Weinheim, Germany, 1999; Chapter 3.4.

(3) Bradford, A. M.; Douglas, G.; Manojlovic′-Muir, L.; Muir, K. W.; Puddephatt, R. J. *Organometallics* **1990**, *9*, 409.

(4) Adams, R. D.; Wu, W. *J. Cluster Sci.* **1991**, *2*, 271.

(5) Adams, R. D.; Captain, B.; Fu, W.; Pellechia, P. J. *Chem. Commun.* **2000**, 937.

10.1021/ic0207000 CCC: $25.00
Published on Web 04/05/2003

Experimental Section

General Data. All reactions were performed under a nitrogen atmosphere, using the standard Schlenk labware techniques. Reagent-grade solvents were dried by the standard procedures and were freshly distilled prior to use. Infrared spectra were recorded on a Nicolet model 5DXBO Fourier transform infrared spectrophotometer. ^{1}H NMR and ^{31}P NMR spectra were recorded on a Varian model Inova 500 spectrometer operating at 500.16 and 202.47 MHz, respectively. ^{31}P NMR spectra were externally referenced against 85% *ortho*-H_3PO_4. Variable-temperature (VT) ^{1}H NMR spectra were determined using the Varian Inova temperature probe that was calibrated with ethylene glycol. Elemental analyses were performed by Desert Analytics (Tucson, AZ). PMe_2Ph, PMe_3, and Me_2S were purchased from Sigma−Aldrich and used without further purification. $PtRu_5(CO)_{16}(\mu_6\text{-C})$ was prepared according to the published procedure.[4] Product separations were performed by thin-layer chromotography (TLC) in air on Analtech 0.25 and 0.5 mm silica gel 60 Å F_{254} glass plates.

Preparation of $PtRu_5(CO)_{15}(PMe_2Ph)(\mu_6\text{-C})$ (2) and $PtRu_5(CO)_{14}(PMe_2Ph)_2(\mu_6\text{-C})$ (3). A quantity of compound **1** (12.6 mg, 0.011 mmol) was allowed to react with 1.2 μL of PMe_2Ph (0.014 mmol) in 15 mL of CH_2Cl_2 at 25 °C for 30 min. The products were separated by TLC in air, using hexane solvent, to yield 3.9 mg of **2** (36%) and 5.2 mg of **3** (45%). Spectral data for **2**: IR ν_{CO} (cm^{-1} in CH_2Cl_2) 2085 (m), 2066 (sh), 2054 (vs), 2037 (vs), 1995 (sh), 1852 (w, br). ^{1}H NMR (in 1,2-dichlorobenzene-d_4) data were collected for a **2a**:**2b** isomer ratio (major isomer to minor isomer) of 7:3 at 25 °C. For isomer **2a**: δ = 1.78 ppm (d, 6H, CH_3, $^2J_{P-H}$ = 10 Hz, $^3J_{Pt-H}$ = 53 Hz); ^{31}P{^{1}H} NMR (in 1,2-dichlorobenzene-d_4) δ = −10.52 ppm ($^1J_{Pt-P}$ = 6084 Hz). For isomer **2b**: ^{1}H NMR (in 1,2-dichlorobenzene-d_4) δ = 1.98 ppm (d, 6H, CH_3, $^2J_{P-H}$ = 10 Hz); ^{31}P{^{1}H} NMR (in 1,2-dichlorobenzene-d_4) δ = 9.51 ppm ($^2J_{Pt-P}$ = 115 Hz). ^{13}CO-enriched ^{13}C NMR (in CD_2Cl_2 at 20 °C) δ = 197 ppm (averaged singlet, J_{C-Pt} = 61 Hz). Anal. Calcd: C, 22.68; H, 0.87. Found: C, 22.92; H, 0.76. Spectral data for **3**: IR ν_{CO} (cm^{-1} in CH_2Cl_2) 2069 (m), 2021 (vs), 1968 (sh), 1811 (w, br). ^{1}H NMR (in 1,2-dichlorobenzene-d_4), for 50% isomer **3a**: δ = 1.85 ppm (d, 6H, CH_3, $^2J_{P-H}$ = 9.8 Hz, $^3J_{Pt-H}$ = 51.0 Hz), δ = 1.51 ppm (d, 6H, CH_3, $^2J_{P-H}$ = 10.8 Hz). For 40% isomer **3b**: δ = 1.94 ppm (d, 6H, CH_3, $^2J_{P-H}$ = 9.5 Hz). For 10% isomer **3c**: δ = 1.75−2.04 ppm (J_{Pt-H} and J_{P-H} were obscured in this region). ^{31}P{^{1}H} NMR (in 1,2-dichlorobenzene-d_4), for isomer **3a**: δ = −13.45 ppm (d, $^1J_{P-Pt}$ = 5999 Hz, J_{P-P} = 8 Hz), δ = 9.62 ppm (d, J_{P-Pt} = 63 Hz, J_{P-P} = 8 Hz). For isomer **3b**: δ = 4.35 ppm (s, $^2J_{Pt-P}$ = 139 Hz). For isomer **3c**: δ = −11.80 ppm (d, $^1J_{Pt-P}$ = 6111 Hz, J_{P-P} = 7 Hz), δ = −1.11 ppm (d, J_{P-P} = 7 Hz). Anal. Calcd: C, 30.46; H, 1.93. Found: C, 30.41; H, 1.89.

Preparation of $PtRu_5(CO)_{15}(PMe_3)(\mu_6\text{-C})$ (4) and $PtRu_5(CO)_{14}(PMe_3)_2(\mu_6\text{-C})$ (5). A quantity of compound **1** (11.0 mg, 0.009 mmol) was allowed to react with 0.9 μL of PMe_3 (0.009 mmol) in 15 mL of CH_2Cl_2 at 25 °C for 40 min. The products were separated by TLC in air, using a hexane solvent, to yield 1.7 mg of **4** (16%) and 1.2 mg of **5** (11%). Spectral data for **4**: IR ν_{CO} (cm^{-1} in CH_2Cl_2) 2085 (m), 2066 (sh), 2054 (vs), 2037 (vs), 1995 (sh), 1852 (w, br). ^{1}H NMR (in 1,2-dichlorobenzene-d_4) data were collected for a **4a**:**4b** isomer ratio (major isomer to minor isomer) of 7:3 at 25 °C. For isomer **4a**: δ = 1.47 ppm (d, 6H, CH_3, $^2J_{P-H}$ = 10.5 Hz, $^3J_{Pt-H}$ = 52 Hz); ^{31}P{^{1}H} NMR (in 1,2-dichlorobenzene-d_4) δ = −21.43 ppm ($^1J_{Pt-P}$ = 6030 Hz). For isomer **4b**: ^{1}H NMR (in 1,2-dichlorobenzene-d_4) δ = 1.64 ppm (d, 6H, CH_3, $^2J_{P-H}$ = 10 Hz); ^{31}P{^{1}H} NMR (in 1,2-dichlorobenzene-d_4) δ = 5.91 ppm ($^2J_{Pt-P}$ = 115 Hz). Spectral data for **5**: IR ν_{CO} (cm^{-1} in CH_2Cl_2) 2069 (m), 2021 (vs), 1968 (sh), 1811 (w, br). ^{1}H NMR (in 1,2-dichlorobenzene-d_4), for isomer **4a**: δ = 1.46 ppm (d, 6H, CH_3, $^2J_{P-H}$ = 9.8 Hz, $^3J_{Pt-H}$ = 51.0 Hz), δ = 1.63 ppm (d, 6H, CH_3, $^2J_{P-H}$ = 10.0 Hz). For isomer **4b**: δ = 1.52 ppm (d, 6H, CH_3, $^2J_{P-H}$ = 15 Hz). For isomer **4c**: δ = 1.48−1.74 ppm (J_{Pt-H} and J_{P-H} were obscured in this region). ^{31}P{^{1}H} NMR (in 1,2-dichlorobenzene-d_4), for 50% isomer: δ = −23.01 ppm (d, $^1J_{P-Pt}$ = 5964 Hz, J_{P-P} = 8 Hz), δ = 1.98 ppm (d, J_{P-Pt} = 67 Hz, J_{P-P} = 8 Hz). For 40% isomer: δ = −1.41 ppm (s, $^2J_{Pt-P}$ = 130 Hz). For 10% isomer: δ = −23.52 ppm (d, $^1J_{Pt-P}$ = 5980 Hz, J_{P-P} = 8 Hz), δ = −7.32 ppm (d, J_{P-P} = 8 Hz).

Preparation of $PtRu_5(CO)_{15}(Me_2S)(\mu_6\text{-C})$ (6). A quantity of compound **1** (13.1 mg, 0.012 mmol) was allowed to react with 11.0 μL of Me_2S (0.15 mmol) in 15 mL of CH_2Cl_2 at 25 °C for 6 h. The product was separated by TLC in air, using a hexane solvent, to yield 6.0 mg of **6** (44%). Spectral data for **6**: IR ν_{CO} (cm^{-1} in hexane) 2087 (m), 2055 (s), 2040 (vs), 2029 (m, sh), 1989 (m, sh), 1835 (w, br). ^{1}H NMR (in CD_2Cl_2 at −40 °C), for 60% isomer **6a**: δ = 2.57 ppm (s, 6H, CH_3, $^3J_{Pt-H}$ = 72 Hz). For 35% isomer **6b**: δ = 2.61 ppm (s, 6H, CH_3). For 5% isomer **6c**: δ = 2.76 ppm (s, 6H, CH_3). Anal. Calcd: C, 18.09; H, 0.36. Found: C, 18.17; H, 0.50.

Crystallographic Analyses. Dark-red crystals of compounds **2** and **3** suitable for diffraction analyses were grown by slow evaporation of solvent from benzene/octane solutions at room temperature. Dark-red crystals of compound **6** suitable for diffraction analysis were grown by slow evaporation of solvent from diethyl ether solution at −20 °C. Crystals **2** and **3** for the diffraction measurements were mounted in thin-walled glass capillaries. Diffraction measurements were made on a Rigaku model AFC6S fully automated four-circle diffractometer, using graphite-monochromated Mo Kα radiation. The unit cells of the crystals were determined and refined from 15 randomly selected reflections that were obtained using the AFC6 automatic search, center, index, and least-squares routines. All data processing was performed on a Silicon-Graphics model INDIGO^2 Workstation, using the TEXSAN structure-solving program library obtained from the Molecular Structure Corporation (The Woodlands, TX). Neutral atom scattering factors were calculated by the standard procedures.[6a] Anomalous dispersion corrections were applied to all non-hydrogen atoms.[6b] Lorentz/polarization (Lp) corrections were applied to the data for each structure. Full-matrix least-squares refinements minimized the function: $\sum_{hkl} w(|F_o| - |F_c|)^2$, where $w = 1/\sigma^2(F)$, $\sigma(F) = \sigma(F_o^2)/(2F_o)$, and $\sigma(F_o^2) = [\sigma(I_{raw})^2 + (0.06I_{net})^2]^{1/2}$/Lp. Both structures were solved by a combination of direct methods (SIR 92) and difference Fourier syntheses.

A crystal of **6** was glued onto the end of a thin glass fiber. X-ray intensity data were measured at 293 K using a Bruker model SMART APEX CCD-based diffractometer that employed Mo Kα radiation (λ = 0.71073 Å). The raw data frames were integrated with the SAINT+ program. Corrections for Lp effects were also applied by SAINT.[7] An empirical absorption correction, which was based on the multiple measurement of equivalent reflections, was applied using the program SADABS. The structure was solved by a combination of direct methods and difference Fourier syntheses and refined by full-matrix least-squares calculations on F^2, using the SHELXTL software package.[8] Crystal data, data collection parameters, and the results of the analyses are listed in Table 1.

(6) (a) *International Tables for X-ray Crystallography*; Kynoch Press: Birmingham, England, 1975; Vol. IV, pp 99−101, Table 2.2B. (b) In ref 6a, pp 149−150, Table 2.3.1.
(7) *SAINT+*, Version 6.2; Bruker Analytical X-ray System, Inc.: Madison, WI, 1997.
(8) Sheldrick, G. M. *SHELXTL*, Version 6.1; Bruker Analytical X-ray Systems, Inc.: Madison, WI, 2000.

Table 1. Crystallographic Data for Compounds **2**, **3**, and **6**

	2	**3**	**6**
formula	$PtRu_5PO_{15}C_{24}H_{11}$	$PtRu_5P_2O_{14}C_{37}H_{28}$	$PtRu_5SO_{15}C_{18}H_6$
fw	1270.76	1459.01	2389.46
cryst syst	orthorhombic	monoclinic	monoclinic
a (Å)	44.897(5)	9.407(1)	18.820(2)
b (Å)	14.590(2)	25.955(7)	17.652(2)
c (Å)	10.208(2)	9.980(1)	18.756(2)
α (°)	90	90	90
β (°)	90	113.41(1)	114.952(2)
γ (°)	90	90	90.
V (Å^3)	6687(2)	2236.0(7)	5649.4(12)
space group	*Pna*2$_1$ (No. 33)	*P*2$_1$/*m* (No. 11)	*P*2$_1$/*c* (No. 14)
Z	8	2	8
ρ_{calc} (g/cm^3)	2.52	2.17	2.81
μ (Mo Kα) (mm^{-1})	6.466	4.882	7.679
temp (°C)	20	20	20
$2\theta_{max}$ (°)	44	46	52
no. of observations	3203 ($I > 3\sigma$)	2637 ($I > 3\sigma$)	9524 ($I > 2\sigma$)
no. of variables	440	287	725
GOF	1.67	1.30	1.026
max shift in final cycle	0.07	0.00	0.002
residuals:[a] *R*; R_w	0.058; 0.080	0.034; 0.046	0.025,0.055
abs correction	Difabs	Difabs	SADABS
transm coeff: max;min	1.00;0.35	1.00;0.45	1.00;0.60
largest peak in final diff. map (e$^-$/Å^3)	1.36	0.97	1.30

[a] $R = \sum_{hkl}(||F_{obs}| - |F_{calc}||)/\sum_{hkl}|F_{obs}|$; $R_w = [\sum_{hkl}w(|F_{obs}| - |F_{calc}|)^2/\sum_{hkl}wF_{obs}^2]^{1/2}$, where $w = 1/\sigma^2(F_{obs})$; GOF $= [\sum_{hkl}(w(|F_{obs}| - |F_{calc}|))^2/(n_{data} - n_{vari})]^{1/2}$.

NMR Calculations. Line-shape analyses were performed on a Gateway personal computer using the EXCHANGE program that was written by R. E. D. McClung of the Department of Chemistry, University of Alberta (Edmonton, Alberta, Canada). For compound **2**, exchange rates were determined at nine different temperatures in the temperature range of 25−130 °C. The activation parameters were determined from a best-fit Eyring plot, using the Microsoft Excel 97 program: $\Delta H^{\ddagger} = 15.1(3)$ kcal/mol, $\Delta S^{\ddagger} = -7.7(9)$ cal/(mol·K), and $\Delta G_{298} = 17.4(6)$ kcal/mol for the transformation of the major isomer to the minor isomer, and $\Delta H^{\ddagger} = 14.5(3)$ kcal/mol and $\Delta S^{\ddagger} = -11.4(9)$ cal/(mol·K) for the transformation of the minor isomer to the major isomer. The thermodynamic parameters were derived from a ln *K* vs 1/*T* plot of the equilibrium constant *K* (major isomer **2a**/minor isomer **2b**),determined from population analyses that were determined by peak integrations at five different temperatures in the range from −5 °C to 25 °C: $\Delta H° = 0.58(8)$ kcal/mol and $\Delta S° = 3.7(3)$ cal/(mol·K).

For compound **4**, exchange rates were determined at 10 different temperatures in the temperature range of 20−160 °C. The activation parameters were determined from a best-fit Eyring plot using the Microsoft Excel 97 program: $\Delta H^{\ddagger} = 14.0(1)$ kcal/mol, $\Delta S^{\ddagger} = -10.7(4)$ cal/(mol·K), and $\Delta G_{298} = 17.2(2)$ kcal/mol for the transformation of the major isomer to the minor isomer, and $\Delta H^{\ddagger} = 13.0(1)$ kcal/mol and $\Delta S^{\ddagger} = -15.1(4)$ cal/(mol·K) for the transformation of the minor isomer to the major isomer. The thermodynamic parameters were derived from a ln *K* vs 1/*T* plot of the equilibrium constant *K* (major isomer **4a**/minor isomer **4b**) determined at five different temperatures in the range from −10 °C to 25 °C: $\Delta H° = 0.97(15)$ kcal/mol and $\Delta S° = 4.4(5)$ cal/(mol·K). For compound **6**, exchange rates were determined at six different temperatures in the range from −40 °C to 15 °C. The activation parameters were determined from a best-fit Eyring plot, using the Microsoft Excel 97 program: $\Delta H^{\ddagger} = 18(1)$ kcal/mol, $\Delta S^{\ddagger} = 21(5)$ cal/(mol·K), and $\Delta G_{298} = 12(2)$ kcal/mol for the transformation of the major isomer to the minor isomer. The thermodynamic parameters were derived from a ln *K* vs 1/*T* plot of the equilibrium constant *K* (major isomer **6a**/minor isomer **6b**) determined at five different temperatures in the range from −80 °C to −30 °C: $\Delta H° = 0.96(5)$ kcal/mol and $\Delta S° = 3.6(2)$ cal/(mol·K).

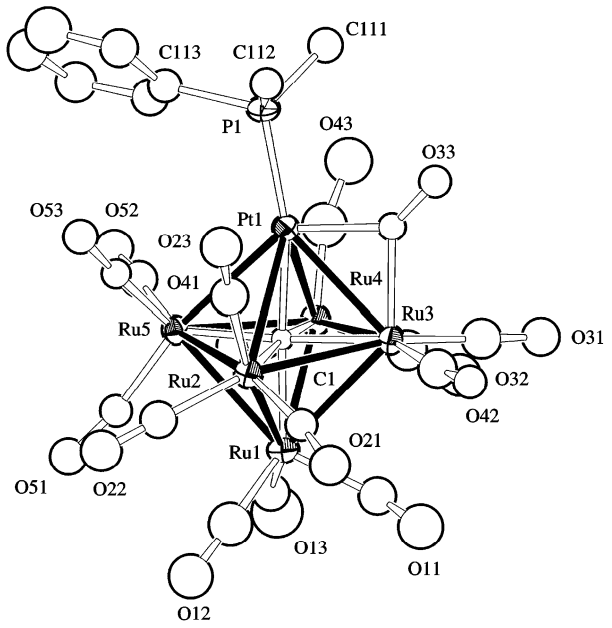

Figure 1. ORTEP diagram of the molecular structure of $PtRu_5(CO)_{15}(PMe_2Ph)(\mu_6\text{-}C)$, **2** (isomer **2a**), showing 40% probability thermal ellipsoids.

Results and Discussion

The reaction of the platinum−ruthenium cluster **1** with PMe_2Ph yielded the mono- and disubstituted derivatives $PtRu_5(CO)_{15}(PMe_2Ph)(\mu_6\text{-}C)$ (**2**) and $PtRu_5(CO)_{14}(PMe_2Ph)_2(\mu_6\text{-}C)$ (**3**), in yields of 36% and 45%, respectively.[5] The molecular structures of **2** and **3** are shown in Figures 1 and 2, respectively. Selected interatomic bond distances and bond angles are listed in Tables 2 and 3. Both compounds are

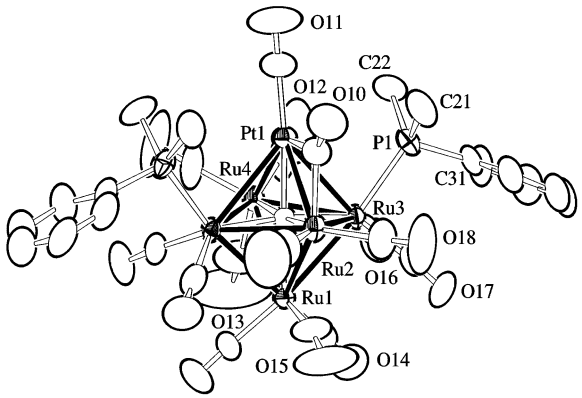

Figure 2. ORTEP diagram of the molecular structure of $PtRu_5(CO)_{14}(PMe_2Ph)_2(\mu_6\text{-C})$, **3**, showing 40% probability thermal ellipsoids.

Table 2. Selected Intramolecular Distances and Angles for $PtRu_5(CO)_{15}(PMe_2Ph)(\mu_6\text{-C})$ (Isomer **2a**)[a]

	Distances (Å)		
Pt(1)−P(1)	2.26(1)	Pt(2)−P(2)	2.27(1)
Pt(1)−Ru(2)	3.058(4)	Pt(2)−Ru(7)	2.951(4)
Pt(1)−Ru(3)	2.773(4)	Pt(2)−Ru(8)	2.930(4)
Pt(1)−Ru(4)	2.949(4)	Pt(2)−Ru(10)	2.758(3)
Pt(1)−Ru(5)	2.888(3)	Ru(6)−Ru(7)	2.823(5)
Ru(1)−Ru(2)	2.819(5)	Ru(6)−Ru(8)	2.899(5)
Ru(1)−Ru(4)	2.819(5)	Ru(6)−Ru(9)	2.824(5)
Ru(1)−Ru(5)	2.920(5)	Ru(6)−Ru(10)	2.979(5)
Ru(2)−Ru(3)	2.923(5)	Ru(7)−Ru(8)	2.895(5)
Ru(2)−Ru(5)	2.862(5)	Ru(7)−Ru(10)	2.937(5)
Ru(3)−Ru(4)	2.921(5)	Ru(8)−Ru(9)	2.875(6)
Ru(4)−Ru(5)	2.895(5)	Ru(9)−Ru(10)	2.907(6)
O(av)−C(av)	1.21(1)	O(av)−C(av)	1.19(1)
	Angles (deg)		
Ru(3)−Pt(1)−P(1)	144.5(3)	Ru(10)−Pt(2)−P(2)	145.4(4)
Ru(5)−Pt(1)−P(1)	123.5(3)	Ru(8)−Pt(2)−P(2)	123.6(3)
Ru(2)−Pt(1)−P(1)	134.3(4)	Ru(7)−Pt(2)−P(2)	132.5(3)

[a] Estimated standard deviations in the least significant figure are given in parentheses.

Table 3. Selected Intramolecular Distances and Angles for $PtRu_5(CO)_{14}(PMe_2Ph)_2(\mu_6\text{-C})$ (**3**)[a]

	Distances (Å)		
Ru(3)−P(1)	2.344(2)	Ru(1)−Ru(3)	2.8194(8)
Pt(1)−Ru(2)	2.780(1)	Ru(1)−Ru(4)	2.965(1)
Pt(1)−Ru(3)	3.0327(7)	Ru(2)−Ru(3)	2.9271(8)
Pt(1)−Ru(4)	2.8643(8)	Ru(3)−Ru(4)	2.9087(8)
Ru(1)−Ru(2)	2.956(1)	O(av)−C(av)	1.16(1)
	Angles (deg)		
Pt(1)−Ru(3)−P(1)	81.60(6)	Ru(4)−Ru(3)−P(1)	114.94(6)
Ru(2)−Ru(3)−P(1)	109.12(6)		

[a] Estimated standard deviations in the least significant figure are given in parentheses.

structurally similar to $PtRu_5(CO)_{16}(\mu_6\text{-C})$[4] and consist of an octahedral cluster containing one Pt and five Ru atoms with a single carbido carbon atom in the center. Compound **2** contains two crystallographically independent molecules in the solid state. Both molecules are structurally similar and have a PMe_2Ph ligand terminally coordinated to the Pt atom: Pt(1)−P(1) = 2.26(1) Å, Pt(2)−P(2) = 2.27(1) Å. There is one carbonyl ligand that bridges one of the Pt−Ru bonds, Pt(1)−Ru(3) = 2.773(4) Å; Pt(2)−Ru(10) = 2.758(3) Å, which is the shortest Pt−Ru bond in the molecule. Because of steric interactions with the bridging CO ligand, the phosphine ligand is leaning toward the Ru atom on the opposite side of the molecule: Ru(5)−Pt(1)−P(1) = 123.5(3)°, Ru(8)−Pt(2)−P(2) = 123.6(3)°.

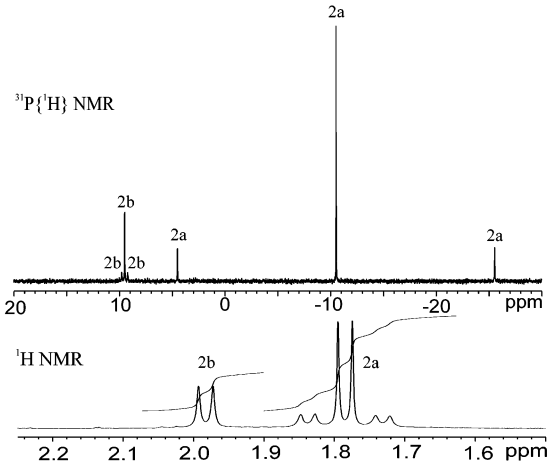

Figure 3. ^1H and $^{31}P\{^1H\}$ NMR spectra of compound **2** at room temperature in 1,2-$C_6D_4Cl_2$ solvent.

Compound **3** contains a crystallograpically imposed reflection symmetry. The Pt atom, the Ru atoms (Ru(1), Ru(2), and Ru(4)), the carbido ligand, and the bridging carbonyl ligand all lie on the reflection plane. The two PMe_2Ph ligands are both coordinated to Ru atoms adjacent to the Pt atom and are related by the reflection symmetry in the solid-state structure. The bridging carbonyl ligand bridges one of the Pt−Ru bonds, which, similar to that in **2**, is the shortest Pt−Ru bond in the molecule (2.780(1) Å).

The ^{31}P and ^1H NMR spectra of **2** show that the compound exists as a mixture of two isomers in a 7:3 ratio in solution at 25 °C (see Figure 3). The ^{31}P NMR resonance of the major isomer **2a**, $\delta = -10.52$ ppm, shows large coupling ($^1J_{Pt-P} = 6084$ Hz) to the Pt atom, indicating that the Pt and P atoms are mutually bonded. In contrast, the small ^{195}Pt coupling ($^2J_{Pt-P} = 115$ Hz) to the phosphorus resonance of the minor isomer **2b**, $\delta = 9.51$ ppm, indicates that the P atom is not bonded to the Pt atom but is, instead, coordinated to one of the neighboring Ru atoms. The thermodynamic parameters for the equilibrium $K = [\mathbf{2a}]/[\mathbf{2b}]$ were derived from population analyses determined by peak integrations at five different temperatures in the range from −5 °C to 25 °C: $\Delta H° = 0.58(8)$ kcal/mol and $\Delta S° = 3.7(3)$ cal/(mol·K).

The NMR assignments for the structures of isomers **2a** and **2b** are also supported by the ^{31}P and ^1H NMR spectra of compound **3**, which shows that this compound exists as a mixture of three isomers in solution, see Figure 4. One isomer, **3b**, shows only a single phosphorus resonance, with a small $^{195}Pt-^{31}P$ coupling of 139 Hz. This resonance is assigned to the isomer, as found in the solid state, that has the equivalent phosphine ligands coordinated to the Ru atoms. The major isomer, **3a**, and a second minor isomer, **3c**, both show phosphorus resonances with large $^{195}Pt-^{31}P$ coupling; $^1J_{Pt-P} = 5999$ Hz (**3a**) and $^1J_{Pt-P} = 6111$ Hz (minor), indicating that one phosphine ligand is coordinated to the Pt atom in each isomer. Isomer **3a** exhibits a second resonance with small $^{195}Pt-^{31}P$ coupling, $^2J_{Pt-P} = 63$ Hz. No $^{195}Pt-^{31}P$ coupling to the second phosphorus resonance was observed for isomer **3c**. It is proposed that one

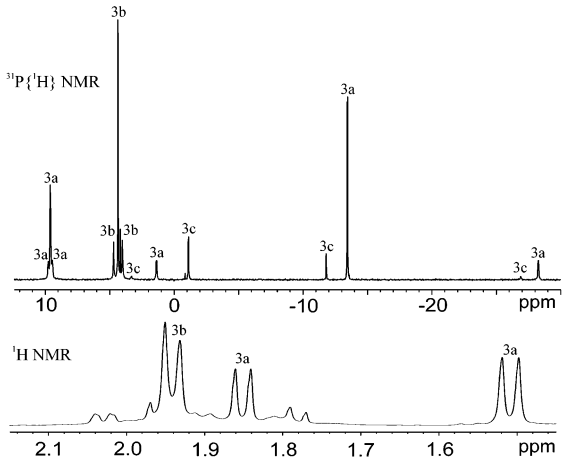

Figure 4. ^1H and $^{31}P\{^1H\}$ NMR spectra of compound **3** at room temperature in 1,2-$C_6D_4Cl_2$ solvent.

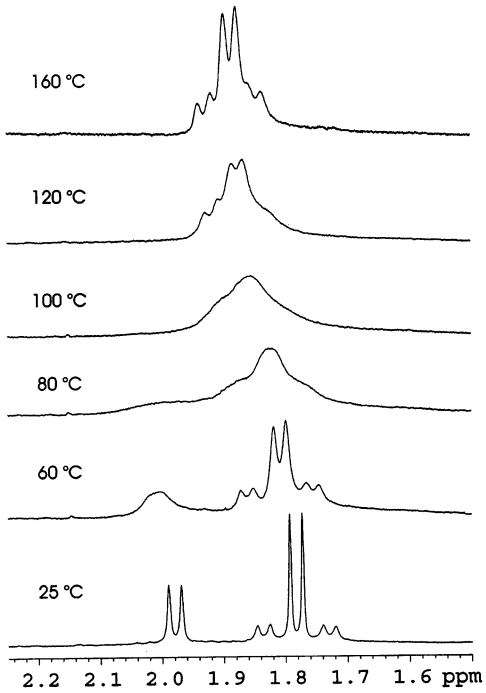

Figure 5. ^1H NMR spectra of compound **2** at various temperatures in 1,2-$C_6D_4Cl_2$ solvent.

PMe_2Ph ligand is coordinated to the Pt atom and one PMe_2-Ph ligand is coordinated to a Ru atom in each of these isomers.

The ^1H NMR spectra of the phosphine methyl resonances of **2** at various temperatures are shown in Figure 5. At 25 °C, two resonances are observed: $\delta = 1.78$ ppm (d, 6H, CH_3, $^2J_{P-H} = 10$ Hz, $^3J_{Pt-H} = 53$ Hz) (isomer **2a**) and $\delta = 1.98$ ppm (d, 6H, CH_3, $^2J_{P-H} = 10$ Hz) (isomer **2b**). Isomer **2a** shows significant $^{195}Pt-^1H$ coupling, whereas no $^{195}Pt-^1H$ coupling is observed for the **2b** isomer. This is consistent with our interpretation of the structures of the **2a** and **2b** isomers, on the basis of the ^{31}P NMR spectra of **2** (see above). It was observed that the resonances of both isomers broaden and coalesce, reversibly, as the temperature is raised, and appear as a resharpened doublet with ^{195}Pt satellites in the averaged spectrum at 160 °C. The $^{195}Pt-^1H$ coupling of 41 Hz observed at 160 °C is equal to the weighted average of the $^{195}Pt-^1H$ coupling of the two isomers at this temperature. These spectra confirm the existence of a dynamical isomerization process by which the phosphine ligand interchanges coordination sites between the Pt atom and one of the Ru atoms in compound **2**. The observation of the ^{195}Pt coupling in the averaged spectra confirms that the process occurs intramolecularly.[9] The exchange broadened spectra were simulated by line-shape calculations that have provided exchange rates and, in turn, activation parameters for the process: $\Delta G^{\ddagger}_{298} = 17.4(6)$ kcal/mol, $\Delta H^{\ddagger} = 15.1(3)$ kcal/mol, and $\Delta S^{\ddagger} = -7.7(9)$ cal/(mol·K) for the transformation of **2a** to **2b**, and $\Delta H^{\ddagger} = 14.5(3)$ kcal/mol and $\Delta S^{\ddagger} = -11.4(9)$ cal/(mol·K) for the transformation of **2b** to **2a**.

A mechanism to explain these spectral changes is shown in Scheme 1. The dynamical isomerization between isomers **2a** and **2b** can be explained by a shift of the phosphine ligand from the Pt atom to one of the neighboring Ru atoms. It is proposed that the phosphine ligand is shifted to the Ru atom positioned opposite to the Ru atom containing the bridging carbonyl ligand. The process may be initiated by a series of CO ligand shifts that pass through an intermediate such as **A** shown in Scheme 1. To form intermediate **A** from isomer **2a**, the bridging CO ligand is shifted to a terminal position on the Pt atom and two terminal CO ligands on Ru atoms are shifted to bridging positions across two adjacent Ru−Ru bonds. The structure of intermediate **A** is analogous to that of the compound $PtRu_5(CO)_{14}(PPh_2CH_2CH_2PPh_2)(\mu_6\text{-}C)$ recently reported by Shapley[10] in which both P atoms of the $PPh_2CH_2CH_2PPh_2$ chelate are coordinated to the Pt atom. The transformation to isomer **2b** is completed by a shift of the phosphine ligand from the Pt atom to the Ru atom. The phosphine ligand must, at some point, be simultaneously bonded to both the Pt and Ru atoms, as in intermediate **B** shown in Scheme 1. There are very few examples of bridging coordination of tertiary phosphines in metal complexes; however, Werner recently reported some of the first examples in the complexes $[(acac)Rh(\mu\text{-}PMe_3)(\mu\text{-}CPh_2)_2Rh(acac)]$[11] and $[ClRh(\mu\text{-}PMe_3)(\mu\text{-}CPh_2)_2RhCl]_2$,[12] which contain PMe_3 ligands that are bridging two Rh atoms. To complete the exchange, the bridging CO ligands are shifted to terminal positions, as indicated by the arrows in intermediate **B**, and a terminal CO ligand is moved into a bridging position across the same Pt−Ru bond that contained the bridging CO ligand in isomer **2a**. The process is reversible.[13] A singlet observed at 197 ppm in the ^{13}C NMR spectrum at room temperature with Pt−C coupling of 61 Hz indicates that the CO ligands are rapidly exchanging without dissociation, even at this low temperature.

(9) Jesson, J. P.; Muetterties, E. L. In *Dynamic Nuclear Magnetic Resonance Spectroscopy*; Jackman, L., Cotton, F. A., Eds.; Academic Press: New York, 1975, Chapter 8.
(10) Lee, K.; Shapley, J. R. *Organometallics* **1998**, *17*, 3020.
(11) Pechmann, T.; Brandt, C. D.; Werner, H. *Angew. Chem., Int. Ed.* **2000**, *39*, 3909.
(12) Pechmann, T.; Brandt, C. D.; Roger, C.; Werner, H. *Angew. Chem., Int. Ed.* **2002**, *41*, 2301.
(13) Heaton, B. H.; Strona, L.; Martinengo, S. *J. Organomet. Chem.* **1981**, *215*, 415.

Scheme 1 Proposed Mechanism for the Isomerization of Two Isomers of Compound **2** by Intramolecular Shifts of the Phosphine and Carbonyl Ligands between the Metal Atoms[a]

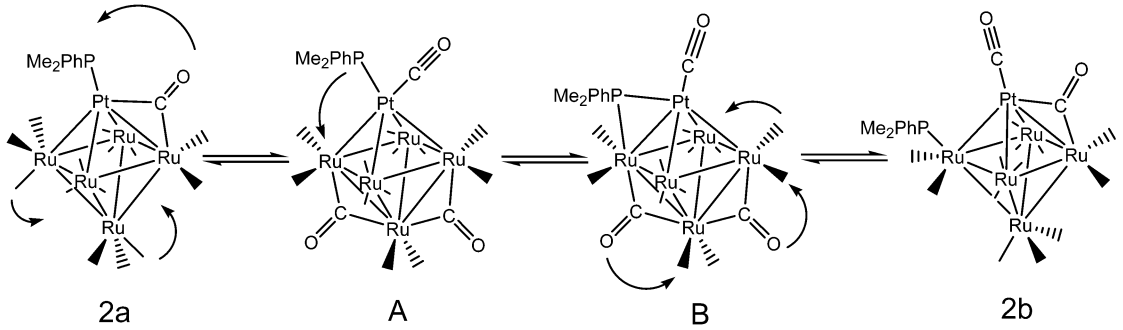

[a] The carbon atom in the center of the cluster is omitted for clarity.

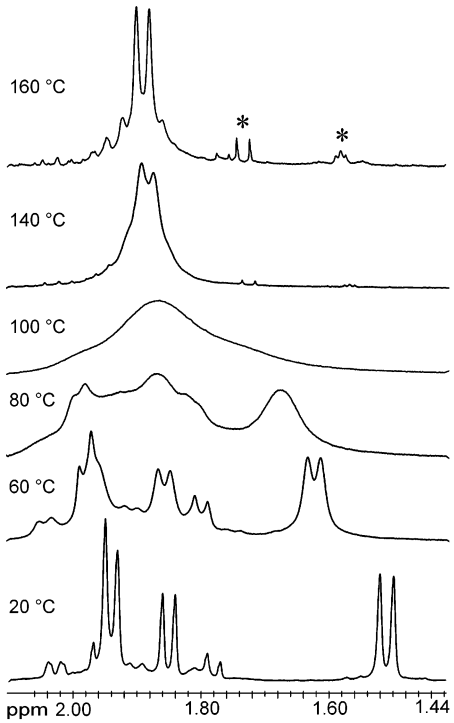

Figure 6. ^{1}H NMR spectra of compound **3** at various temperatures in 1,2-$C_6D_4Cl_2$ solvent. Resonances marked with an asterisk are traces of unidentified decomposition products in the sample.

The ^{1}H NMR spectra of the methyl resonances of compound **3** at various temperatures are shown in Figure 6. At 25 °C, three resonances are observed that are attributed to three isomers: the major isomer, **3a** (δ = 1.85 ppm (d, 6H, CH_3, $^{2}J_{P-H}$ = 9.8 Hz, $^{3}J_{Pt-H}$ = 51.0 Hz), δ = 1.51 ppm (d, 6H, CH_3, $^{2}J_{P-H}$ = 10.8 Hz)), isomer **3b** (δ = 1.94 ppm (d, 6H, CH_3, $^{2}J_{P-H}$ = 9.5 Hz)), and the minor isomer, **3c** (δ = 1.75−2.04 ppm). Two isomers (the 50% and 10% isomers) show significant ^{195}Pt−^{1}H coupling; no ^{195}Pt−^{1}H coupling was observed for the 40% isomer. This is consistent with our observations of the ^{31}P NMR spectra of **3** (see above). It was observed that the resonances of all three isomers broaden and coalesce, reversibly, as the temperature is raised; however, most importantly, ^{195}Pt satellites are observed on the resonances in the averaged spectrum at 170 °C. These spectra confirm the existence of a dynamical isomerization processes through which the phosphine ligand interchanges coordination sites between the Pt atom and the neighboring Ru atoms in **3**, and the observation of the ^{195}Pt coupling in the averaged spectra confirms that the process is intramolecular.[9] Because of the complexity produced by the presence of three actively interconverting isomers of compound **3** in solution, it was not possible to obtain accurate activation parameters for the rearrangements.

For comparison, we also prepared the compounds $PtRu_5(CO)_{15}(PMe_3)(\mu_6\text{-}C)$ (**4**) and $PtRu_5(CO)_{14}(PMe_3)_2(\mu_6\text{-}C)$ (**5**) and investigated their ligand dynamics. Compounds **4** and **5** were characterized by a combination of IR and NMR spectroscopy. Compound **4** behaves similarly in solution to compound **2**; that is, it exists in solution as a mixture of two isomers, in a 7:3 ratio at 25 °C, and the fast-exchange limit was reached at 160 °C with ^{195}Pt−^{1}H coupling being maintained. The exchange-broadened spectra were also simulated by line-shape calculations, which provided exchange rates and, in turn, activation parameters for the process: $\Delta G^{\ddagger}_{298}$ = 17.2(2) kcal/mol, $\Delta H^{\ddagger}$= 14.0(1) kcal/mol, and $\Delta S^{\ddagger}$ = −10.7(4) cal/(mol·K) for the transformation of the major isomer to the minor isomer, and $\Delta H^{\ddagger}$ = 13.0(1) kcal/mol and $\Delta S^{\ddagger}$ = −15.1(4) cal/(mol·K) for the transformation of the minor isomer to the major isomer. Similar to compound **3**, compound **5** also exists in solution as a mixture of three isomers that broaden, coalesce, and average as the temperature is raised. ^{195}Pt−^{1}H coupling is maintained in the fast-exchange limit.

We also prepared and investigated the ligand dynamics of $PtRu_5(CO)_{15}(Me_2S)(\mu_6\text{-}C)$ **(6)**. Compound **6** was obtained in 44% yield from the reaction of **1** with Me_2S. Compound **6** was characterized by a combination of IR, NMR, and single-crystal X-ray diffraction analyses. Compound **6** contains two crystallographically independent molecules in the asymmetric crystal unit. Both molecules are structurally similar, and an ORTEP diagram of the molecular structure of one of these molecules is shown in Figure 7. Selected interatomic bond distances and bond angles are listed in Table 4. The cluster of **6** is similar to that of **2**. The Me_2S ligand is terminally coordinated to the Pt atom: Pt(1)−S(1) = 2.2926(14) Å, Pt(2)−S(2) = 2.2963(14) Å. As in compounds **2** and **3**, there is one bridging carbonyl ligand that bridges the shortest Pt−Ru bond in the cluster: Pt(1)−Ru(3) = 2.7451(5) Å; Pt(2)−Ru(8) = 2.7466(5) Å. Interestingly, the ^{1}H NMR spectrum of compound **6** at −40 °C shows three resonances of unequal intensities for the methyl

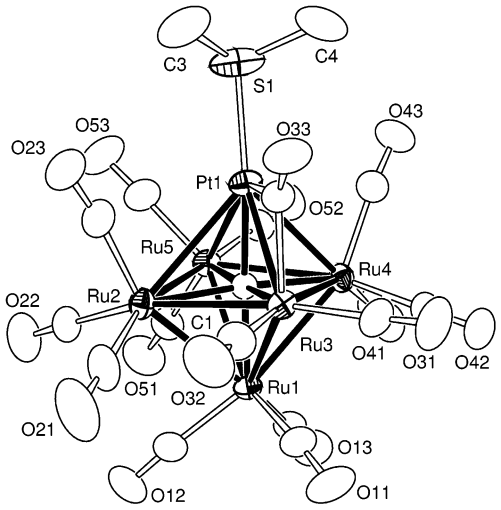

Figure 7. ORTEP diagram of the molecular structure of $PtRu_5(CO)_{15}(Me_2S)(\mu_6\text{-}C)$, **6** (isomer **6a**), showing 40% probability thermal ellipsoids.

Table 4. Selected Intramolecular Distances and Angles for $PtRu_5(CO)_{15}(Me_2S)(\mu_6\text{-}C)$ (Isomer **6a**)[a]

	Distances (Å)		
Pt(1)−S(1)	2.2926(14)	Pt(2)−S(2)	2.2963(14)
Pt(1)−Ru(2)	3.0254(5)	Pt(2)−Ru(7)	3.0069(5)
Pt(1)−Ru(3)	2.7451(5)	Pt(2)−Ru(8)	2.7466(5)
Pt(1)−Ru(4)	2.9214(4)	Pt(2)−Ru(9)	2.9365(5)
Pt(1)−Ru(5)	2.9308(4)	Pt(2)−Ru(10)	2.9270(5)
Ru(1)−Ru(2)	2.8261(5)	Ru(6)−Ru(7)	2.8189(5)
Ru(1)−Ru(3)	2.9752(5)	Ru(6)−Ru(8)	2.9562(6)
Ru(1)−Ru(4)	2.8270(5)	Ru(6)−Ru(9)	2.8319(6)
Ru(1)−Ru(5)	2.8956(6)	Ru(6)−Ru(10)	2.9214(6)
Ru(2)−Ru(3)	2.9239(6)	Ru(7)−Ru(8)	2.9160(6)
Ru(2)−Ru(5)	2.8529(5)	Ru(7)−Ru(10)	2.8664(5)
Ru(3)−Ru(4)	2.9774(6)	Ru(8)−Ru(9)	2.9625(6)
Ru(4)−Ru(5)	2.8859(6)	Ru(9)−Ru(10)	2.8912(6)
O(av)−C(av)	1.13(1)	O(av)−C(av)	1.14(1)
	Angles (deg)		
Ru(3)−Pt(1)−S(1)	146.93(4)	Ru(8)−Pt(2)−S(2)	147.24(4)
Ru(5)−Pt(1)−S(1)	120.88(4)	Ru(10)−Pt(2)−S(2)	120.03(4)
Ru(2)−Pt(1)−S(1)	135.34(5)	Ru(7)−Pt(2)−S(2)	130.68(5)

[a] Estimated standard deviations in the least significant figure are given in parentheses.

groups, indicating that **6** exists as a mixture of three isomers in solution. The resonance at $\delta = 2.57$ ppm (60% abundance), isomer **6a**, shows coupling ($^3J_{Pt-H} = 72$ Hz) to the Pt atom, which suggests that this isomer has the structure found in the solid state. The two other resonances, at $\delta = 2.61$ and 2.76 ppm, exhibit no coupling to the Pt atom. These resonances are assigned to isomers **6b** and **6c**, respectively, in which the Me_2S ligand is bonded to a Ru atom.

VT ^{1}H NMR spectra of the methyl resonances of compound **6** are shown in Figure 8. It was observed that the resonances of two of the isomers, **6a** and **6b** ($\delta = 2.57$ and 2.61 ppm), broaden and coalesce, reversibly, as the temperature is raised, with ^{195}Pt−^{1}H coupling ($^3J_{Pt-H} = 40$ Hz) being observed in the averaged spectrum at 15 °C. The resonance at $\delta = 2.76$ ppm, isomer **6c** (5% abundance), broadens and collapses into the baseline at ∼0 °C. Coalescence with the other resonances was not observed; however, a 2D EXSY ^{1}H NMR spectrum for **6** at −10 °C, Figure 9, shows strong cross peaks between isomer **6c** and the averaged resonance of isomers **6a** and **6b**, thus confirming its exchange, albeit

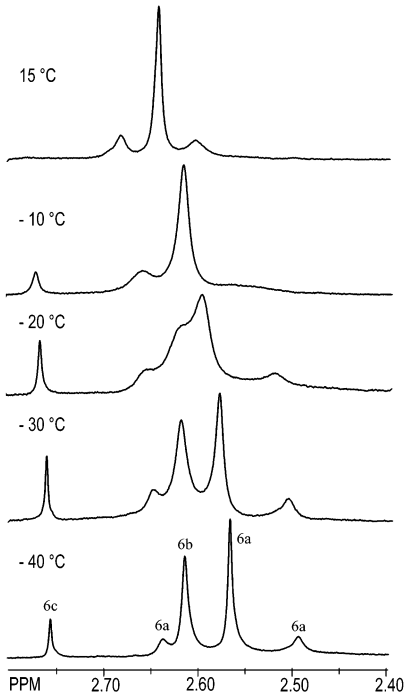

Figure 8. ^{1}H NMR spectra of compound **6** at various temperatures in CD_2Cl_2 solvent.

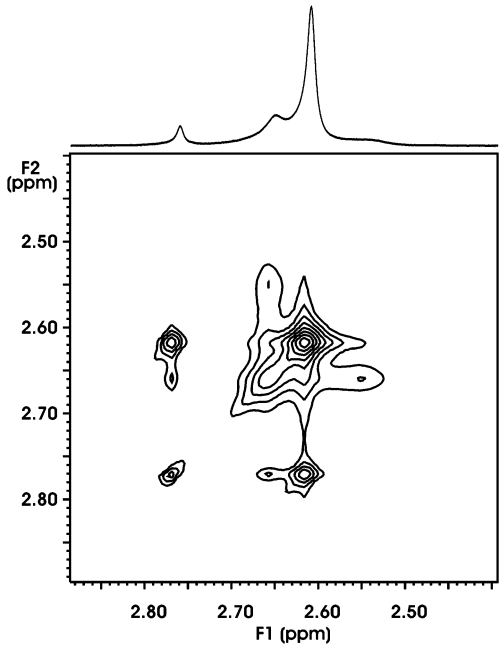

Figure 9. Two-dimensional EXSY NOESY ^{1}H NMR spectrum of **6** at −10 °C in CD_2Cl_2 solvent.

much slower, with them. Isomer **6b** is believed to be structurally analogous to isomer **2b**, having the Me_2S ligand on a Ru atom adjacent to the Pt atom, and the mechanism of exchange of the Me_2S ligand between the metal atoms of isomers **6a** and **6b** is proposed to be analogous to that observed for the two isomers of **2** and **4**. The binding site of the Me_2S ligand in isomer **6c** has not been established; however, we suspect that it may be on the Ru atom located trans to the Pt atom for the following reason. The VT NMR data indicate that the exchange of isomer **6c** with isomers

6a and **6b** is much slower than that between isomers **6a** and **6b**. We believe that, if the Me_2S ligand was positioned on any of the Ru atoms adjacent to the Pt atom, then its exchange with isomers **6a** and **6b** would be energetically similar to the exchange between isomers **6a** and **6b**, because all isomerizations would involve intermediates with an Me_2S ligand bridging a Pt−Ru bond. However, an intramolecular Me_2S metal−metal exchange involving an isomer with the Me_2S ligand on a Ru atom located trans to the Pt atom would require an intermediate that has the Me_2S ligand bridging a Ru−Ru bond. We cannot determine a priori if this would be more or less favorable than a Pt−Ru bridged intermediate, but it should be different.

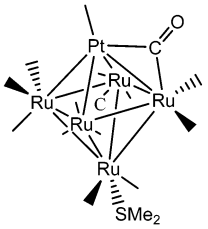

We did not have enough exchange-rate data to determine the activation parameters for the isomerization of isomer **6c** with isomers **6a** and **6b**; however, there was a sufficient amount of rate data from line-shape analyses to determine the activation parameters for the **6a** → **6b** isomerization. As can be anticipated from the much lower temperatures for the exchange of isomers **6a** and **6b**, the activation parameters are also much lower: $\Delta G^{\ddagger}_{298} = 12(2)$ kcal/mol, $\Delta H^{\ddagger} = 18(1)$ kcal/mol, and $\Delta S^{\ddagger} = 21(5)$ cal/(mol·K) versus $\Delta G^{\ddagger}_{298}$ **2a** → **2b** and $\Delta G^{\ddagger}_{298}$ **4a** → **4b** (which are equal to 17.4(6) and 17.2(2) kcal/mol, respectively).

The relatively low barrier for the **6a** → **6b** isomerization may be due to differences in bonding of the bridging ligand in an intermediate. In particular, in a phosphine-bridged intermediate, the phosphine ligand can donate only two electrons for simultaneous coordination to the two metal atoms, i.e., a 3c−2e bond is formed in a species such as that shown in intermediate **C**. However, in a Me_2S bridged intermediate, such as that observed in intermediate **D**, the S atom can donate four electrons, using its two lone pairs of electrons to form two donor−acceptor bonds. This should be more stable than the bridged tertiary phosphine and, thus,

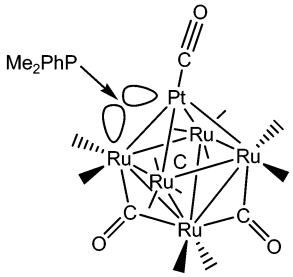

C

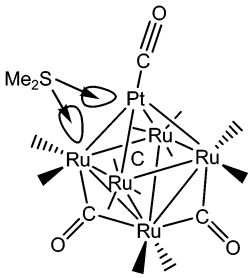

D

facilitate the interconversion between isomers **6a** and **6b**. There are many examples of polynuclear metal complexes that contain bridging thioether ligands.[14] There are very few examples of complexes containing bridging tertiary phosphine ligands.[11,12]

Conclusion

In this report, we have described some of the first examples of a facile intramolecular metal−metal exchange for phosphine and thioether ligands. The thioether ligand is able to migrate between the metal atoms much faster that the tertiary phosphine ligand in the $PtRu_5$ cluster. Because of the widespread occurrence of phosphine and thioether ligands in polynuclear metal complexes, it may be anticipated that similar intramolecular processes will be found to occur in other metal cluster complexes as well.

Acknowledgment. These studies were supported by the Division of Chemical Sciences of the Office of Basic Energy Sciences of the U.S. Department of Energy (under Grant No. DE-FG02-00ER14980) and by the USC Nanocenter.

Supporting Information Available: X-ray crystallographic data in CIF format for compounds **2**, **3**, and **6** with details of the structure solutions and refinement. This material is available free of charge via the Internet at http://pubs.acs.org.

IC0207000

(14) (a) Adams, R. D.; Belinski, J. A.; Chen, L. *Organometallics* **1992**, *11*, 4104. (b) Boorman, P. M.; Moynihan, K. J.; Oakley, R. T. *Chem. Commun.* **1982**, 899. (c) Cotton, F. A.; Duraj, S. A.; Roth, W. J. *Acta Crystallogr., Sect. C: Cryst. Struct. Commun.* **1985**, *41*, 878. (d) Boorman, P. M.; Moynihan, K. J.; Richardson, J. F. *Inorg. Chem.* **1988**, *27*, 3207. (e) Boorman, P. M.; Gao, X.; Freeman, G. K. W.; Faot, J. F. *J. Chem. Soc., Dalton Trans.* **1991**, 115. (f) Boorman, P. M.; Gao, X.; Parvez, M. *J. Chem. Soc., Dalton Trans.* **1992**, 25. (g) Ball, J. M.; Boorman, P. M.; Moynihan, K. J. *Can. J. Chem.* **1990**, *68*, 685.